Energy Harvesting from the Beating Heart by a Mass Imbalance Oscillation Generator

A. Zurbuchen,[1] A. Pfenniger,[1,4] A. Stahel,[4] C. T. Stoeck,[3] S. Vandenberghe,[1]
V. M. Koch,[4] and Rolf Vogel[1,2,5]

[1]ARTORG Center for Biomedical Engineering Research, University of Bern, 3010 Bern, Switzerland; [2]Department of Cardiology, Solothurner Spitäler, 4500 Solothurn, Switzerland; [3]Institute for Biomedical Engineering, University and ETH Zurich, 8092 Zurich, Switzerland; [4]Engineering and Information Technology, Bern University of Applied Sciences, 2501 Biel, Switzerland; and [5]Department of Cardiology, Bern University Hospital, Bern, Switzerland

Associate Editor Xiaoxiang Zheng oversaw the review of this article.

Abstract—Energy-harvesting devices attract wide interest as power supplies of today's medical implants. Their long lifetime will spare patients from repeated surgical interventions. They also offer the opportunity to further miniaturize existing implants such as pacemakers, defibrillators or recorders of bio signals. A mass imbalance oscillation generator, which consists of a clockwork from a commercially available automatic wrist watch, was used as energy harvesting device to convert the kinetic energy from the cardiac wall motion to electrical energy. An MRI-based motion analysis of the left ventricle revealed basal regions to be energetically most favorable for the rotating unbalance of our harvester. A mathematical model was developed as a tool for optimizing the device's configuration. The model was validated by an *in vitro* experiment where an arm robot accelerated the harvesting device by reproducing the cardiac motion. Furthermore, in an *in vivo* experiment, the device was affixed onto a sheep heart for 1 h. The generated power in both experiments—*in vitro* (30 μW) and *in vivo* (16.7 μW)—is sufficient to power modern pacemakers.

Keywords—Scavenging, Automatic power-generating system, Power supplies, Cardiac wall motion, MRI, Unbalance, Wrist watch.

INTRODUCTION

Over the last few years, medical implants have rapidly gained importance and are continuously extending their field of application. Most of them rely on internal primary batteries, which have become a well-established and reliable power supply. Batteries however have a major disadvantage: a limited capacity and therefore a limited life span. Recent efforts aimed at increasing their energy density have shown very small effect.[10,12] Whereas the dimensions of electronic circuits are constantly reduced, batteries often account for an important percentage of volume, and weight of today's medical implants. Therefore, energy harvesting is a promising alternative to batteries. Different technologies have been investigated to extract energy from various sites and sources of the body[16] as for example the knee,[13] the chemical reaction of glucose and oxygen in dedicated fuel cells,[7] the body movements using nanowires,[14] the body heat[24] or the ventricular wall motion.[1,6,22]

Using the cardiac contraction as a power source for energy harvesting can be beneficial in many ways. Regardless of a person's activity, the heart's contractions are regular with displacements in the range of centimeters. The cardiac muscle is highly enduring with more than 1.8 billion heart cycles during a lifetime of 70 years at an averaged heart rate of 70 beats per minute. This makes it a very reliable power source that may also offer the opportunity to power medical implants such as a pacemaker—a device dedicated to the heart. The power consumption of the latest pacemakers has been further reduced to 8 μW.[26] However, the energy required depends on the device's activity, and therefore the lifespan of battery-driven pacemakers usually vary between 6 and 12 years. In order to replace a depleted battery, a complete device replacement becomes necessary. Particularly young people might therefore undergo repeated surgical interventions, each with the risk of complications. Moreover, the leads of pacemakers and defibrillators have a

Address correspondence to Rolf Vogel, Department of Cardiology, Solothurner Spitäler, 4500 Solothurn, Switzerland. Electronic mail: rolf.vogel@spital.so.ch

considerable risk of failure.[8] These leads would become obsolete if the primary battery of pacemakers was replaced by an "inexhaustible" power supply near the heart, thereby improving the patient's quality of life significantly.

In this research work, we make use of the automatic watch mechanism to harvest the energy of a person's heartbeat. Our approach is divided in three parts: First, a modified wrist watch is used in an *in vivo* experiment to demonstrate the feasibility. Since an automatic wrist watch is originally designed for arm motion and not intended for implantation onto the heart, its energy harvesting capabilities are far from optimal when operated by cardiac contractions. Therefore, it is the second task of this study to describe the physical behavior of the harvesting technique by a mathematical model. Such a model allows a systematic study of the influence of different design parameters on output energy. Finally, we performed an *in vitro* experiment with an arm robot to validate the results of the mathematical model.

MATERIALS AND METHODS

Test Setup

The mechanism of an automatic wrist watch has been used in the watch industry for years. It is a well-established technique to harvest energy from a person's wrist by transforming mechanical into electrical energy. The arm's motion is converted into rotation by means of an eccentric oscillating weight. In our particular case, this mass in turn winds a spring which accumulates the mechanical energy. When a certain threshold has been reached, the spring energy is released to drive an electromagnetic generator during a few milliseconds, producing electrical pulses referred as "triggered impulses". The generated electrical energy is then stored in an accumulator or capacitor in order to supply the watch even during periods of inactivity.

A first prototype has been constructed by using the clockwork ETA 204 (ETA SA, Switzerland) from a commercially available automatic wrist watch. In order to reduce the total weight, all unnecessary parts have been removed, namely the wristband, the steel housing, the dial, the indicators, and the gear wheels responsible for displaying the time and date. The modified wrist watch—including the electromagnetic generator (MG205, Kinetron B.V., the Netherlands), the oscillation weight (3.5 g), and a bracket—was placed in a custom-made housing covered by the original glass lid. This custom made housing provides six eyelets in order to sew it onto the epicardium, the outer side of the heart muscle (Fig. 5). It was manufactured by 3D printing (Alaris30, Objet Ltd., Israel) out of polymer VeroWhite FullCure830 (Objet Ltd.). The final weight of the modified device is 16.7 g. We later refer to this device as mass imbalance oscillation generator (MIOG). No further modifications were done to the prototype during or between the experiments.

For all experiments the MIOG operates with a 330 Ω load resistance and a data acquisition setup (SCB-68 and DAQCard-6062E, National Instruments Corp., USA). LabVIEW (National Instruments) was used to measure and process the sampled voltage signal (Fig. 1). Our program comprises an edge detector to count the impulses of the generator.

Heart Motion Analysis

MRI Tagging Analysis

With regard to harvesting energy from the cardiac motion, it is of great interest to identify the epicardial sites with the most promising motion spectrum. Cardiac magnetic resonance imaging (MRI) was used to assess cardiac motion *in vivo*. Imaging was performed on a 1.5 T Philips MRI system (Achieva, Philips Healthcare, the Netherlands). Data were acquired in one healthy volunteer (30 year old male). Written informed consent was obtained according to the
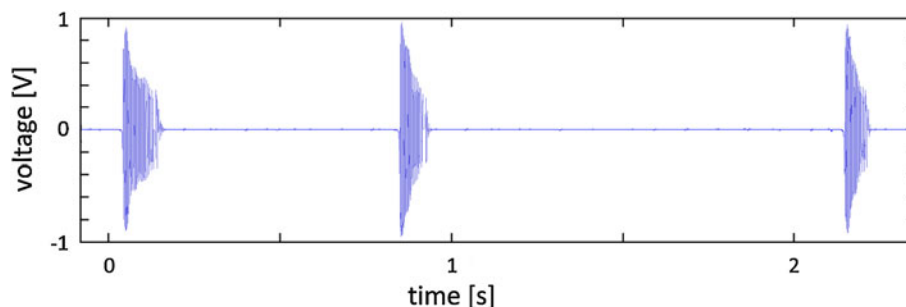
FIGURE 1. Output signal of the prototype generator. The data were acquired during the *in vitro* experiment at the basal site. A single impulse provides a mean energy of 43.8 μJ.

institutional guidelines prior to the exam. 3D Cardiac tagging images covering the entire left ventricle were acquired using Complementary SPAtial Modulation of Magnetization (CSPAMM[4]) preparation in combination with an ECG triggered multi-shot gradient echo sequence employing echo planar imaging (EPI) read-outs. Tagging preparation immediately followed detection of the *R*-wave. Sequence parameters were as follows: spatial resolution $3.9 \times 7.7 \times 7.7$ mm³, field of view $108 \times 108 \times 108$ mm³, TR/TE: 6.9/3.2 ms, tag-line distance: 7 mm, temporal resolution 24.5 ms, 29 heart phases/frames per cycle (fpc). In order to achieve constant signal intensity over the cardiac cycle a flip angle sweep was used.[21] As recommended by Rutz et al.[18] three stacks with orthogonal line tagging pattern were acquired in three consecutive breath holds with a duration of 18 heartbeats each. Breath hold level was controlled using a respiratory navigator placed on the right hemi diaphragm (gating window 15 mm). Navigator data was used to correct for offsets in stack position during image reconstruction. Mid-wall contours were drawn in short axis view and tracked over time. Tracking was performed in phase domain using the peak combination harmonic phase (HARP)[11,19] algorithm implemented in an in-house programmed software (IDL). Displacement information required for simulations was retrieved from tracked contour points. For every vertex translational as well as rotational motion during the cardiac cycle was computed. Although the MIOG experiences accelerations in all six degrees of freedom (DOF), accelerations along the device's rotation axis have no direct influence on the oscillating weight. The calculations in the following motion analyses are based on translational displacements rather than accelerations in order to avoid discretization errors caused by differentiation of trajectories with low temporal resolution.

Translational Motion Analysis

In a first approach, we used the principal component analysis (PCA) to compute the translational displacement variability for each tagged point. The procedure for a single point $P_{t,v,z}$ over time t for a specific depth z along the long axis of the left ventricle and vertex v,

$$\mathbf{P}_{v,z} = \begin{bmatrix} P_{1,t=1,v,z} & P_{1,t=2,v,z} & P_{1,t=fpc,v,z} \\ P_{2,t=1,v,z} & P_{2,t=2,v,z} & \cdots & P_{2,t=fpc,v,z} \\ P_{3,t=1,v,z} & P_{3,t=2,v,z} & P_{3,t=fpc,v,z} \end{bmatrix},$$
$$v = [1 \ldots 72], \quad z = [1 \ldots 11] \tag{1}$$

involves detrending the data,

$$\mathbf{Pmean}_{v,z} = \mathbf{P}_{v,z} - mean\{\mathbf{P}_{v,z} | t = 1, 2, 3 \ldots fpc\} \tag{2}$$

building the covariance matrix

$$\mathbf{C} = \text{cov}(\mathbf{Pmean}_{v,z}) \tag{3}$$

and the singular value decomposition of the covariance matrix $\mathbf{C}$. This yields the product of three matrices that are known as the eigenvector matrix $\mathbf{U}$, the diagonal eigenvalues matrix $\mathbf{S}$ and the transposed eigenvector matrix $\mathbf{V^T}$:

$$\mathbf{USV^T} = svd(\mathbf{C}) \tag{4}$$

The first principal component (the first eigenvector) points in the direction of the largest variance. As an example, the PCA of points on an ellipse would identify its major and minor axis with its first and second eigenvector, respectively. Therefore, the strongest motion amplitude of a point on the left ventricle is found along the first principle component. The sum of the eigenvalues represents the total amount of variation of a point's motion during one heart cycle.

The second approach, i.e., the translational analysis, considers only forces in the device's *x–y*-plane (device plane, normal to the unbalance rotation axis, Fig. 2). Accelerations in *z*-direction only affect the unbalance's bearing, i.e. the bearings' rolling resistance and can therefore be neglected for this analysis. The main task is to find the traveled distance in this plane during one cardiac cycle. Since the orientation of the device changes over time, a normal vector perpendicular to the heart's surface is computed for every time step. This is done by the cross product of secants from the opposing neighboring points (Fig. 3). Assuming a rigid mechanical coupling between the heart and the device, the constructed normal vector and the device's *z*-axis coincide. To calculate path fragments without
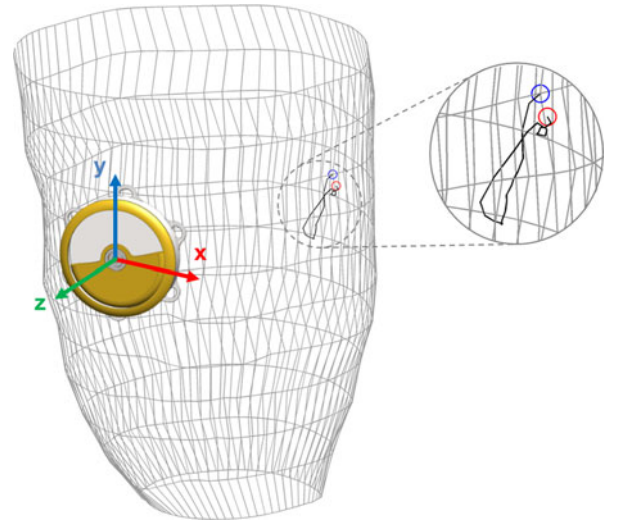
FIGURE 2. Prototype generator on MRI tagging grid of the left ventricle and a trajectory of a single vertex over time. The circles highlight the starting- (blue) and end-point (red) of the motion.

z-components, the path of a vertex was therefore projected on the device plane for every time step. The sum of all these partial displacements yields a total amount of displacement projected on the heart surface.

Rotational Motion Analysis

The myocardial torsion induces a rotation in the device's *x–y*-plane at a particular implantation site (Fig. 3, red vertex), which affects the motion of the oscillating weight. The amount of rotation in the device plane d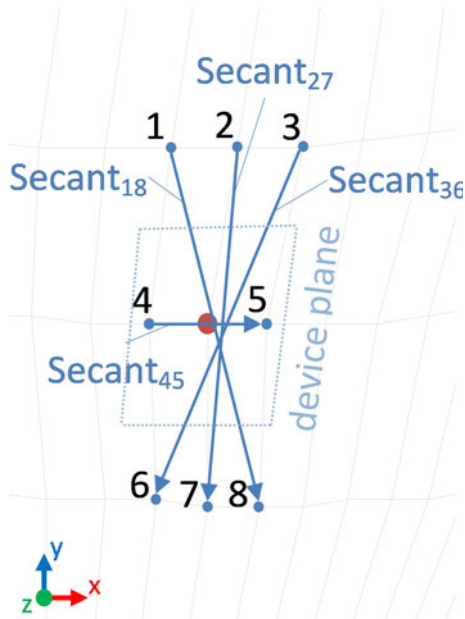uring one heart cycle is determined by the sum of incremental rotations between consecutive time steps. The incremental rotation is derived from the rotation of neighboring points around the normal vector between two time steps. We used the secants of opposing neighboring points (1–8, 2–7 and 3–6) to determine this absolute angular deflection by averaging the angular deviation of each secant. Secant 4–5 proved to be an insufficient indicator of the rotational behavior and was therefore excluded from these calculations.

FIGURE 3. The neighboring points of a vertex (red spot) are used to calculate the translational and angular displacement.

Computational Analysis

Based on the device specifications, a mathematical model was developed to compute the motion of the unbalance for a given three-dimensional heart motion. The unbalance was modeled by a single mass point attached on a rigid and weightless beam, whose motion is constrained to a circular path. Among the accelerations caused by the myocardial contraction (three translational, three rotational), the translational acceleration along the *z*-axis does not influence the behavior of the oscillating weight.

The general setup is given by the free-body diagram (Fig. 4) showing the unbalance in the 3D space with the point S as its center of mass. The reference frame illustrates the origin of the unbalance's housing in the inertial frame. Its orientation is described by the time-dependent transformation matrix **u**:

$$\mathbf{u}(\mathbf{t}) = \begin{pmatrix} \vec{u}_1 & \vec{u}_2 & \vec{u}_3 \end{pmatrix} = \begin{pmatrix} u_{1x} & u_{2x} & u_{3x} \\ u_{1y} & u_{2y} & u_{3y} \\ u_{1z} & u_{2z} & u_{3z} \end{pmatrix} \quad (5)$$
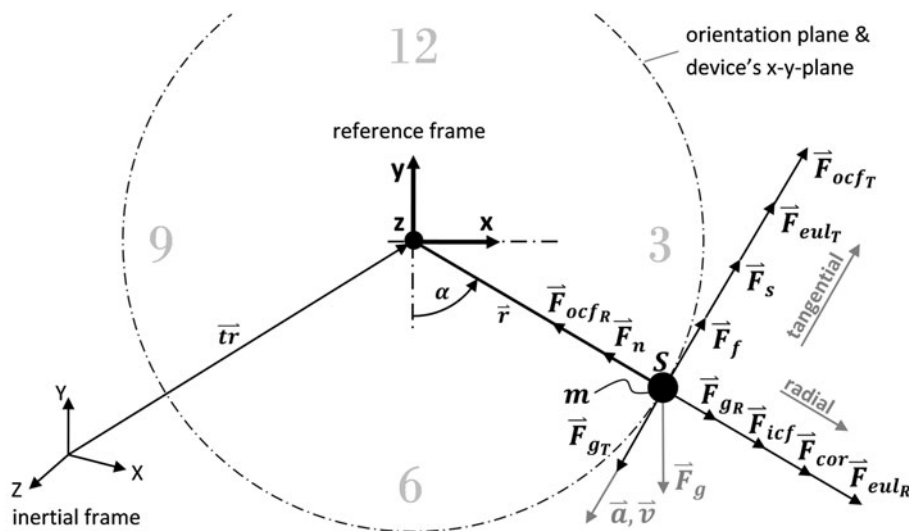

FIGURE 4. Free-body diagram with radial and tangential acting forces.

In the reference frame the x-axis points towards 3 o'clock, the y-axis towards 12 o'clock and the z-axis along the rotation axis perpendicular to the housing. Any pose (position and orientation) of the device can be described by combining the position vector $\vec{tr}$ with the orientation matrix $\mathbf{u}$.

The energy produced by the excited pendulum is examined by means of a numerical solution of its equation of motion. According to Newton's second law, the problem can be described in the inertial frame by the sum of all forces

$$m\vec{a} = \sum \vec{F} \tag{6}$$

and by the sum of all moments:

$$J\alpha'' = mr^2\alpha'' = \sum \vec{M} \tag{7}$$

For the mathematical formulation in the accelerated reference frame, real, and fictitious forces have to be taken into account. The real forces are the gravity $F_g = -mg$, the friction force F_f and the spring force F_s.

The friction force F_f in the unbalance's ball bearing is divided into kinetic ($\mu_k = 0.005$) and static ($\mu_s = 0.05$) friction force for a given tangential velocity threshold. F_f always points opposite to the rotation direction and results from the normal force F_n acting radially on the bearing.

$$F_f = \begin{cases} -\mu_k F_n \text{sign}(\alpha') & \text{for } |r\alpha'| \geq 1 \text{ mm s}^{-1} \\ -\mu_s F_n \text{sign}(\alpha') & \text{for } |r\alpha'| < 1 \text{ mm s}^{-1} \end{cases} \tag{8}$$

The counter force of the spring F_s, which is responsible for the mechanical energy transmission to the electromagnetic generator, plays a key role in this analysis. Manufacturer specifications report a linear increase of spring force with displacement.[15] When the cumulated rotation α_{cum} of our unbalance reaches 2.5 radians, the spring reaches its maximum torque of $M_{spring} = 90$ μNm and unloads the stored energy to the generator. To compute α_{cum} in the numerical model we integrated the absolute angular velocity over time.

$$\alpha_{cum} = \int abs(\alpha')dt$$
$$F_s = -M_{spring}/r \ \text{mod}\,(\alpha_{cum}, 2.5)/2.5 \ \text{sign}(\alpha') \tag{9}$$

By formulating the system in the accelerated reference frame, fictitious forces acting on all masses in non-inertial frames had to be introduced.[3] Therefore, the mathematical model includes centrifugal forces which arise from the angular velocity of the reference frame $\vec{\Omega}$

$$F_{ocf} = \left| m\vec{\Omega} \times \left(\vec{\Omega} \times \vec{r} \right) \right| \tag{10}$$

and from the angular velocity of the pendulum α'

$$F_{icf} = mr(\alpha')^2 \tag{11}$$

and are subsequently denoted by outer and inner centrifugal force, respectively.

Further fictitious forces are the Coriolis force

$$F_{cor} = \left| 2m\vec{\Omega} \times \vec{v}_t \right| \quad \text{with} \quad v_t = r\alpha' \tag{12}$$

and the Euler force

$$F_{eul} = \left| m\vec{\Omega}' \times \vec{r} \right| \tag{13}$$

which are caused by angular accelerations $\vec{\Omega}'$.

The inertial force represents the reaction force to the translational motion of a single point on the heart $\vec{tr}$ which was built by considering only the tangential component of the motion vector. Building the external motion trajectory $\vec{tr}$ was part of the in vitro experiment and is explained in ''In Vitro Experiment'' section.

$$F_i = -\left| m\,\vec{tr}'' \right| \tag{14}$$

All the forces are hereby expressed as a function of known quantities, except for the friction, which consists of an unknown and always radially oriented normal force F_n. By separating the free-body diagram (Fig. 4) into tangential (T) and radial (R) components the following system of equations is obtained and can be used to solve for the unknown force F_n:

$$T: \ mr^2\alpha'' = M_g + M_f + M_i + M_{eul} + M_{ocf} + M_s$$
$$R: \ F_n = F_{g_R} + F_{icf} + F_{i_R} + F_{ocf_R} + F_{eul_R} + F_{cor} \tag{15}$$

A vector space transformation is used to separate the original force vectors into tangential or radial components which are denoted by capital T or R indices. However, there are two forces which only influence the radial equilibrium, namely the inner centrifugal force F_{icf} and the Coriolis force F_{cor}. Solving this well-defined system of equations by eliminating the variable F_n results in a second order explicit ordinary differential equation (ODE) for the angular acceleration α''.

$$\alpha'' = \left(M_g + M_f + M_i + M_{eul} + M_{ocf} + M_s \right)/mr^2 \tag{16}$$

To find a numerical solution to this problem we converted this second order equation to a system of first order equations. This system can be integrated by using the classical 4th order Runge–Kutta algorithm with adaptive step size control.

For the validation of the model a total amount of triggered impulses is calculated by dividing the cumulated absolute angular distance α_{cum} by 2.5 radians.

To ensure the quality of the numerical solver's result, different minimal step sizes with various simulation times are tested. The variation between simulations with different step sizes is evaluated by comparing the amount of triggered impulses.

In Vitro Experiment

An arm robot (5 DOF, ±0.1 mm accuracy, Neuronics Katana, Switzerland) was programmed to reproduce the motion of a particular point of a beating human heart. Simulating over several consecutive heartbeat cycles requires a repeatable and closed trajectory as input. Trajectories were obtained from MRI tagging data covering the entire systole and most of diastole. Due to ECG-based triggering of the MRI sequence acquisition, data cannot be recorded at the end of diastole right before occurrence of the next *R*-wave. Therefore, a gap between the starting and the end point of the motion is inevitable. For this experiment we used a built-in function of the robot to close the trajectories. The input coordinates had to be adjusted to avoid artificial excessive motions caused by the interpolation over this gap. Furthermore, trajectories obtained from our MRI tagging analyses showed strong acceleration peaks that could not be reproduced accurately by the robot. The trajectories therefore had to be adapted to the robot's capabilities. Most important, due to the limited DOF of the robot, the trajectories were simplified to translational movements only (*x*, *y*, and *z*). An optical tracking system (0.15 mm 3D accuracy, 4600 Hz maximum update rate, Optotrak Certus, Northern Digital Inc., USA) was used to capture the robot's end-effector motion with an update rate of 100 Hz. This tracking data of the generator's motion is used as input for the later comparison with our mathematical model.

In Vivo Experiment

The MIOG was used in a study approved by the Swiss Federal Veterinary Office that is in compliance with the Guide for the Care and Use of Laboratory Animals (National Academy of Sciences, 1996). The animal received humane care in compliance with the Guide for the Care and Use of Laboratory Animals. The study was performed on a 65 kg female Swiss alpine sheep during 1 h. After premedication and induction of anesthesia, the animal was intubated and anesthesia was maintained with isoflurane in oxygen (1.6%) and fentanyl (5–10 μg kg^{-1} h^{-1}).[20] The sheep was placed in the right-lateral position. After left anterolateral thoracotomy and pericardiotomy, the MIOG was directly sewn onto the left ventricular, midlateral wall (Fig. 5). In addition, a sponge-like pad was
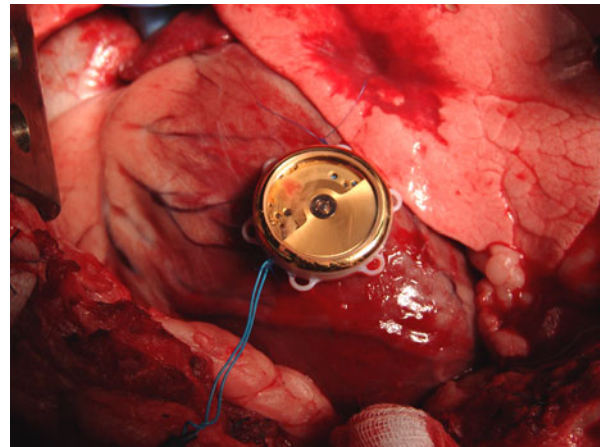

FIGURE 5. The prototype generator sewn (blue threads) onto the sheep's heart using three eyelets of the housing.

glued onto the back of the prototype to enhance the adhesion on the epicardium. This site was chosen for three reasons. First, it was free of relevant coronary arteries. Second, it was not necessary to mobilize the heart, thus preventing venous congestion. And third, the device remained visible throughout the experiment. The surgeons first attached two threads to the myocardial tissue. Then, the device was fixated by using three eyelets of the housing.

RESULTS

Left Ventricular Wall Motion Analysis

First, the variation of translational displacements was investigated using the PCA method that provides easily comparable values, thus simplifying the identification of the segments with the longest trajectories regardless of the motion direction. As illustrated in Fig. 6a, this analysis reveals long trajectories in the basal region, in particular on the lateral side. Furthermore, PCA generates three eigenvectors that span a new coordinate system for each point. The principle component of a given trajectory can now be used to describe the main direction of a motion which for large displacements comprises up to 97% of its total variation. For the most favorable sites, the motion directions show a clear tendency toward a general torsion of the heart along its long-axis. In contrast to the PCA method, where the absolute traveled distances are rather uniformly distributed, there is a greater proportion of large distances in the translational motion analysis (Fig. 6b). Strong movements dominate in the lateral region, in particular at the basal level. The rotational analysis, on the other hand, reveals deviations higher than 27.3° in all segments of the left ventricle (Fig. 6c). In general, rotational motions were
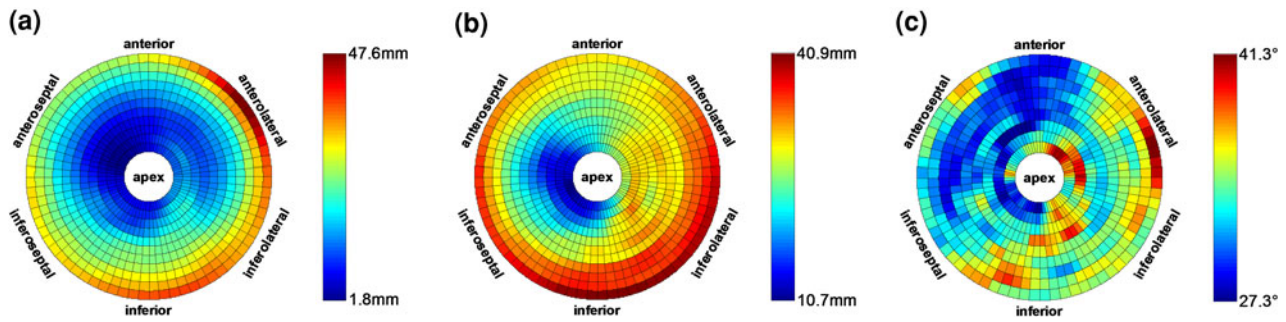
FIGURE 6. Bull's eye plot showing (a) the variation for translational displacements (PCA), (b) the translational displacement, and (c) the rotations coplanar to the epicardial surface. Basal and apical motion data are depicted in the outer and inner circumference of the Bull's eye, respectively.

stronger in inferior and inferolateral segments. Based on these motion analyses, we conclude that the basal-inferolateral region is the best place to harvest energy with a MIOG.
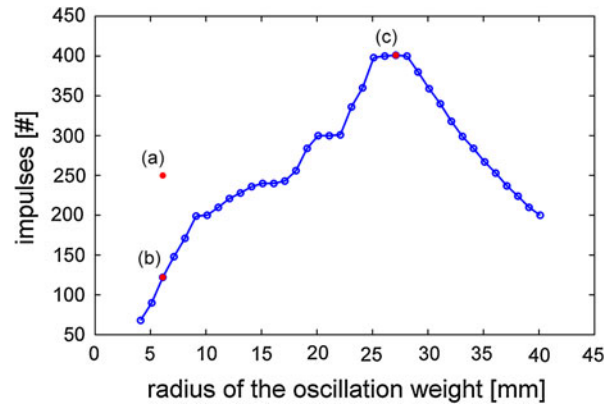
Mathematical Model

For the validation of the mathematical model, we used the trajectories acquired by the optical tracking system during the *in vitro* experiment. The MIOG was therefore stimulated by translational excitations only. Figure 8 illustrates the contribution of each force as a function of time. Since our mathematical model does not compute the output power but rather the number of electric impulses (calculated by dividing the cumulated angle α_{cum} by 2.5 radians), we decided to use this quantity for comparison with the *in vitro* experiment. For identical test conditions, 250 impulses were generated during the *in vitro* experiment, whereas 122 impulses were predicted by the simulation. The consistency of the numerical solver was confirmed by using different step sizes.

We verified the model's ability to predict an optimal configuration for one of the design parameters. To this end, the radius of the oscillation weight was varied from 4.1 to 40.1 mm. As shown in Fig. 7, a maximum of 401 impulses is found at a radius of 27.1 mm.

In Vitro Experiment

The arm robot was programmed to move the MIOG along the trajectory of two different points. The first point was chosen based on the previous motion analysis and was located basally at the inferolateral side. In contrast to this, the second point was selected from the apical level where small translational motions were measured. The robot reproduced 600 heart cycles and thereby accelerated the MIOG during 8 min and 58 s and 7 min and 9 s, respectively. In both experiments, the unbalance had a maximal oscillation amplitude of approximately 20°. The device delivered a

FIGURE 7. Predicted impulses by the mathematical model for different oscillation weight radii. The plot illustrates the number of generated impulses (a) in the *in vitro* experiment, (b) predicted by the mathematical model with the original prototype radius (6.1 mm), and (c) under optimal radius configuration of 27.1 mm.

mean power of 30.0 μW (26.9 μJ per heartbeat) at the basal and 23.2 μW (16.6 μJ per heartbeat) at the apical level.

In Vivo Experiment

During the *in vivo* experiment the sheep had an average heart rate of 90 bpm. Our prototype was affixed to the heart for 1 h. Macroscopically, the sutures affixing the device did not harm the myocardium and there was no obvious abrasion of the epicardial surface. During the experiment, we performed three power measurements for a total time of 18 min and 45 s. During this time the generator produced 330 impulses with a mean power of 16.7 μW that translates into 11.1 μJ per heartbeat.

DISCUSSION

We demonstrated that it is technically feasible to gain energy from the beating heart by means of an

unbalance as it is used to power wrist watches. The mean power generated in *in vivo* tests is sufficient to supply the latest pacemaker designs with power consumption in the range of 8 μW.[26] This was achieved by a few simple modifications of a commercially-available automatic wrist watch without optimization of size, weight or transduction mechanism. To find the energetically favorable spots for a prospective device implantation we investigated the left ventricular wall deformation based on MRI tagging data. Furthermore, we developed and validated a mathematical model which can be used to optimize the harvester with respect to size and power delivery. The proof of concept was demonstrated during a 1-h *in vivo* experiment.

Prototype

Automatic wrist watches are known to have a very long lifetime, but they require occasional servicing. A complex clockwork is required to guarantee accuracy and reliability. Because a lot of today's watches are worn as jewelry, the micro-machined parts not only have to be precise but also need to have an attractive design. Apart from longevity, the requirements of prospective harvesting device are rather different. Harvesting the mechanical motion from the beating heart will be its exclusive task. This will reduce the complexity of the mechanical construction and therefore improve the resistance to wear. Moreover, the encapsulation from any external mechanical stresses and the constant body temperature provide an advantageous implantation site for the device. In the setting of human energy harvesting, we therefore expect a substantially longer lifetime of the MIOG devices without maintenance.

Our first prototype is not yet optimized to be used in conjunction with cardiac motions and may, due to its size and mass, harm the heart or interfere with cardiac function. Ideally, the weight of the housing would be limited to a minimum and the weight and shape of the unbalance would have to be chosen to match with the motion spectrum of the beating heart. Because these parameters change with heart rate, it is essential to find a design that operates within a certain bandwidth. Furthermore, the oscillating weight reacts only to accelerations within its two-dimensional motion plane. Therefore, the optimal harvesting device should be small and contain a dedicated generating mechanism with the ability to efficiently extract energy from a given spectrum of movements.

In order to improve the device's ability to harvest energy over a wide range of excitations, a dynamic adaptation could be envisioned. Similar approaches have been studied in the setting of electromagnetic[25] and piezoelectric[9] generators. Nevertheless, a dynamic adaptation can only be achieved at the cost of some energy (e.g., an actuator is required to modify the device's configuration). Therefore, the challenge is to design an adaptation mechanism consuming a mere fraction of the produced energy.

Operation of a cardiac pacemaker requires an energy management system to buffer the power converted by the generator in a capacitor. This backup unit ensures proper functioning during periods of cardiac malfunction, e.g., arrhythmias or ischemia. Such a management system must be carefully designed to match the final configuration of the harvester and the consuming device.

MRI Tagging for Heart Motion Analysis

MRI tagging was developed to analyze cardiac wall motion mainly in the setting of coronary artery disease.[17] It is well known that the anatomical structure of a heart varies significantly for different individuals. However, in this study we focused on the motion spectrum of one individual. Although MRI tagging is the clinical gold standard to assess the cardiac wall motion, it suffers from certain limitations. First, tagging data reflect points of the middle myocardial layer and do not necessarily reflect the behavior of epicardial points (relative circumferential shortening epicardial, $22 \pm 5\%$; midwall, $30 \pm 5\%$; and endocardial, $44 \pm 6\%$).[2] In addition, it is currently challenging to realize MRI measurements covering multiple R–R intervals so that the starting and the end point of a trajectory coincide due to cardiac triggering and length of breath holding. We therefore had to adjust our trajectories for the simulations which require a continuous periodic function as input.

The calculation of normal vectors and maximal rotating angles relies on neighboring points of adjacent planes at a fixed offset (Fig. 3). Because the vertices in the basal and apical short-axis planes lack three neighboring points, only 9 of 11 short-axis slices were used for the rotational motion analysis (Fig. 6c).

MRI data are acquired in supine position. At present, MRI techniques cannot investigate the influence of various body positions like sitting or standing and activities such as walking or running on cardiac motion and its potential to drive an energy harvester. Such scenarios can only be assessed during *in vivo* experiments.

Experiments and Simulations

During our *in vivo* experiment, the prototype generator experienced the accelerations of a beating heart during 1 h at a constant heart rate of 90 bpm. Despite the size, weight, and limited oscillation amplitude

(±20°), the MIOG harvested 11.1 μJ electric energy per heartbeat from the left ventricular motion. Similar results were reported in a previous study[6] on a mongrel dog heart, however using overdrive pacing. 13 μJ could be harvested per heartbeat at an optimal heart rate of 200 bpm. Reducing the size and weight of the MIOG might help to fit the device to the heart. However, it also might lead to an inefficient pendulum configuration making the prototype insensitive to the heart's contractions. Three other issues can further explain the different output power of our *in vitro* and *in vivo* experiment: First, the fixation of the prototype by a "loose" suture did not ensure rigid coupling and might have dampened the heart's original excitation. Second, the chosen fixation site on the antero-lateral heart wall (Fig. 5) is not ideal for energy harvesting according to our motion analysis. Third, open chest test conditions with reduced intrathoracic pressure deviate from the physiologic situation. This may have influenced cardiac motion and energy production of our device. Furthermore, the impact of the MIOG's mass (16.7 g) on cardiac performance is not known. However, the normal weight of a human heart (360–410 g[5]) often includes epicardial fat accumulations[23] that clearly exceed the mass of our harvesting device. To date, these fat deposits have not been shown to negatively affect cardiac performance.

In contrast to the *in vivo* experiment, the clamp mechanism of the arm robot ensured rigid mechanical contact between the generator and the source of motion. However, the use of an arm robot raised some other issues: First, the trajectory had to be smoothened to overcome the high acceleration peaks found during cardiac contraction. Second, the robot is not designed for reproducing small deflections with high accelerations. Finally, due to the limited DOF of the robot, we could only consider translational motion.

Due to gravity, the oscillating mass of our MIOG will always settle in the position where its potential energy is minimal. To deflect the mass from that one point, it is therefore important to have accelerations whose directions are not aligned with gravity. In both the *in vivo* and the *in vitro* experiment, the amplitude and direction of the heart motion varied sufficiently for the mass to oscillate by approximately ±20°.

An optical tracking system was used to acquire accurate three-dimensional information of the robot's end effector motion. We used a cubic spline interpolation of this trajectory to obtain a twice differentiable function as input to our mathematical model. This interpolation resulted in a slight overshoot for acceleration peaks and might therefore support the unbalance's motion. Because the robot lacks rotational DOF, the mathematical model is not yet validated for rotational components. Therefore, we could not assess the impact of the Coriolis-, Euler-, and outer centrifugal force on the device.
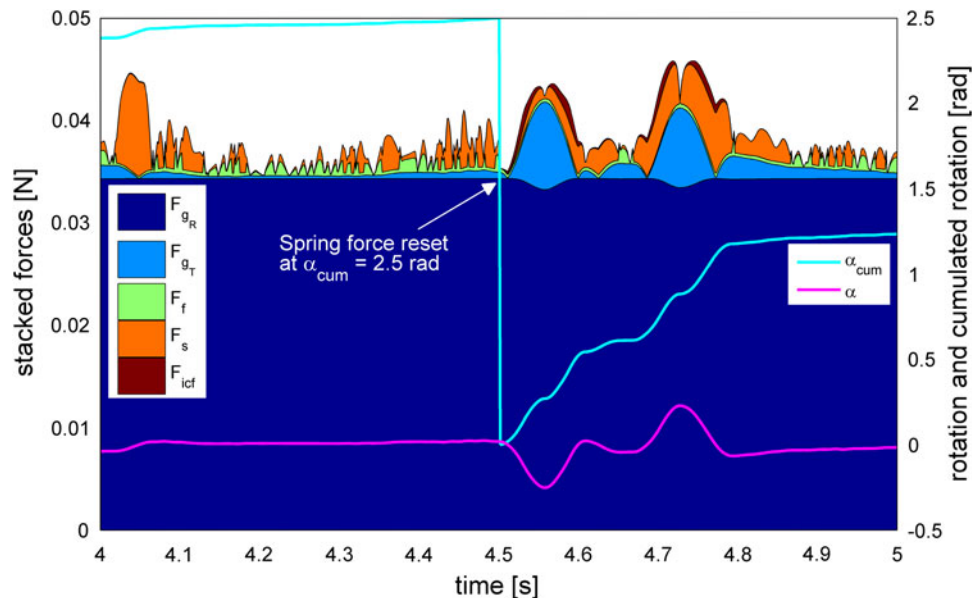
FIGURE 8. Stacked force plot of the mathematical model. α denotes the instantaneous angle of the unbalance. The cumulated angle α_{cum} illustrates the sudden release of the spring at 2.5 rad which sets the spring force F_s to zero. This reduces the torque on the unbalance sufficiently for the driving inertial force F_i (not displayed) to cause larger oscillations again. Their amplitude rapidly decreases as the spring winds up. Above a certain spring force, stick–slip effects become important (the force F_f alternates between kinetic and static friction as modeled in (8)). Immediately after the spring reset, the moving unbalance produces pure kinetic friction in addition to an inner centrifugal force F_{icf}. Furthermore, the plot shows a large contribution of gravity F_{g_R} compared to the other forces.

Our simulations showed that the system is very sensitive to small changes. The unwinding of the spring, which actuated the electromagnetic generator, suddenly decreases the spring force F_s (see Eq. (9) and Fig. 8) and therefore induces a singularity in the model. Furthermore, the friction force constantly changes between kinetic and static friction as a result of the oscillation. These two sources of discontinuities force the solver to strongly lower its step size. In order to make our ODE differentiable, the signum function in both the friction- and spring-equation were replaced by a smooth approximation (arctangent function). This affected the computation time as well as the numerical result and may introduce an error for long time simulations. Since we do not have an analytical solution to our mathematical model, we cannot calculate these deviations.

Moving mechanical parts always lead to friction. It is the watchmaker's aim to reduce this resistance within clockworks to a minimum. However, the friction coefficient of our movement is unknown. Therefore, several reasonable friction coefficients were tested. According to our numerical results, the contribution of the friction force is very small compared to the gravity or the spring force (Fig. 8). Adjusting the friction coefficients therefore caused only insignificant changes.

As shown by preliminary simulations (Fig. 7), the number of generated impulses can be optimized for a given range of radii, regardless of physical (maximum size or weight of the device) and physiological limitations (influence of the radius on the heart). It is one of the main upcoming tasks in this project to conduct a comprehensive analysis of the relevant design parameters in order to determine their influence on power production under the given biologic limitations. We thereby focus on the development of a simulation platform with the overall goal to find the optimal geometry and harvesting method for a certain spectrum of heart motions. This will allow testing different shapes and transduction mechanisms for their efficiency and applicability. Based on the optimal geometry, more efficient prototypes will be constructed and tested within *in vivo* and *in vitro* studies.

CONCLUSION

The beating heart is a potential energy source to supply active implants. Basal areas of the left ventricular myocardium revealed to be target sites to harvest energy by a MIOG. As predicted by the mathematical model, our first prototype without any optimization already generated sufficient energy to supply the latest cardiac pacemaker.

REFERENCES

[1]Amin Karami, M., and D. J. Inman. Powering pacemakers from heartbeat vibrations using linear and nonlinear energy harvesters. *Appl. Phys. Lett.* 100:042901–042901-4, 2012.

[2]Clark, N., N. Reichek, P. Bergey, E. Hoffman, D. Brownson, L. Palmon, and L. Axel. Circumferential myocardial shortening in the normal human left ventricle. Assessment by magnetic resonance imaging using spatial modulation of magnetization. *Circulation* 84:67–74, 1991.

[3]Dankert, J., and H. Dankert. Technische Mechanik: Statik, Festigkeitslehre, Kinematik/Kinetik. Stuttgart: Teubner, 776 pp, 2009.

[4]Fischer, S. E., G. C. McKinnon, S. E. Maier, and P. Boesiger. Improved myocardial tagging contrast. *Magn. Reson. Med.* 30:191–200, 1993.

[5]Geigy Scientific Tables, Vol. 5: Heart and Circulation. West Caldwell, NJ: Ciba Pharmaceutical Co, 1991, 278 pp.

[6]Goto, H., T. Sugiura, Y. Harada, and T. Kazui. Feasibility of using the automatic generating system for quartz watches as a leadless pacemaker power source. *Med. Biol. Eng. Comput.* 37:377–380, 1999.

[7]Kerzenmacher, S., J. Ducrée, R. Zengerle, and F. von Stetten. Energy harvesting by implantable abiotically catalyzed glucose fuel cells. *J. Power Sources* 182:1–17, 2008.

[8]Kleemann, T., T. Becker, K. Doenges, M. Vater, J. Senges, S. Schneider, W. Saggau, U. Weisse, and K. Seidl. Annual rate of transvenous defibrillation lead defects in implantable cardioverter-defibrillators over a period of >10 years. *Circulation* 115:2474–2480, 2007.

[9]Leland, E. S., and P. K. Wright. Resonance tuning of piezoelectric vibration energy scavenging generators using compressive axial preload. *Smart Mater. Struct.* 15:1413–1420, 2006.

[10]Mateu, L., and F. Moll. Review of energy harvesting techniques and applications for microelectronics. *Proc. SPIE* 5837:359–373, 2005.

[11]Osman, N. F., E. R. McVeigh, and J. L. Prince. Imaging heart motion using harmonic phase MRI. *IEEE Trans. Med. Imaging* 19:186–202, 2000.

[12]Paradiso, J. A., and T. Starner. Energy scavenging for mobile and wireless electronics. *IEEE Pervasive Comput.* 4:18–27, 2005.

[13]Platt, S. R., S. Farritor, K. Garvin, and H. Haider. The use of piezoelectric ceramics for electric power generation within orthopedic implants. *IEEE/ASME Trans. Mechatron.* 10:455–461, 2005.

[14]Qin, Y., X. Wang, and Z. L. Wang. Microfibre-nanowire hybrid structure for energy scavenging. *Nature* 451:809–813, 2008.

[15]Reymondin, C.-A. Theorie der Uhrmacherei. Lausanne: CADEV, 2001.

[16]Romero, E., R. O. Warrington, and M. R. Neuman. Energy scavenging sources for biomedical sensors. *Physiol. Meas.* 30:R35–R62, 2009.

[17]Rutz, A. K., R. Manka, S. Kozerke, S. Roas, P. Boesiger, and J. Schwitter. Left ventricular dyssynchrony in patients with left bundle branch block and patients after myocardial infarction: integration of mechanics and viability by cardiac magnetic resonance. *Eur. Heart J.* 30:2117–2127, 2009.

[18]Rutz, A. K., S. Ryf, S. Plein, P. Boesiger, and S. Kozerke. Accelerated whole-heart 3D CSPAMM for myocardial motion quantification. *Magn. Reson. Med.* 59:755–763, 2008.

[19]Ryf, S., J. Tsao, J. Schwitter, A. Stuessi, and P. Boesiger. Peak-combination HARP: a method to correct for phase errors in HARP. *JMRI-J. Magn. Reson. Imaging* 20:874–880, 2004.

[20]Schauvliege, S., K. Narine, S. Bouchez, D. Desmet, V. Van Parys, G. Van Nooten, and F. Gasthuys. Refined anaesthesia for implantation of engineered experimental aortic valves in the pulmonary artery using a right heart bypass in sheep. *Lab. Anim.* 40:341–352, 2006.

[21]Stuber, M., S. Fischer, M. Scheidegger, and P. Boesiger. Slice Following in Cardiac Imaging with Optimized RF Pulse Angles, New York, 1993.

[22]Tashiro, R., N. Kabei, K. Katayama, E. Tsuboi, and K. Tsuchiya. Development of an electrostatic generator for a cardiac pacemaker that harnesses the ventricular wall motion. *J. Artif. Organs* 5:239–245, 2002.

[23]Thanassoulis, G., J. M. Massaro, U. Hoffmann, A. A. Mahabadi, R. S. Vasan, C. J. O'Donnell, and C. S. Fox. Prevalence, distribution, and risk factor correlates of high pericardial and intrathoracic fat depots in the Framingham heart study. *Circ. Cardiovasc. Imaging* 3:559–566, 2010.

[24]Wang, Z., V. Leonov, P. Fiorini, and C. Van Hoof. Realization of a wearable miniaturized thermoelectric generator for human body applications. *Sens. Actuators A* 156:95–102, 2009.

[25]Wischke, M., M. Masur, F. Goldschmidtboeing, and P. Woias. Piezoelectrically tunable electromagnetic vibration harvester, 2010. doi:10.1109/MEMSYS.2010.5442427.

[26]Wong, L. S., S. Hossain, A. Ta, J. Edvinsson, D. H. Rivas, and H. Naas. A very low-power CMOS mixed-signal IC for implantable pacemaker applications. *IEEE J. Solid-State Circuits* 39:2446–2456, 2004.